HHS Public Access

Author manuscript

Invest Radiol. Author manuscript; available in PMC 2022 December 01.

Published in final edited form as:

Invest Radiol. 2021 December 01; 56(12): 845–853. doi:10.1097/RLI.0000000000000796.

A Pilot Study of Multidimensional Diffusion MRI for Assessment of Tissue Heterogeneity in Prostate Cancer

Björn J. Langbein, MD[*,†,‡], **Filip Szczepankiewicz, PhD**[*,‡,§], **Carl-Fredrik Westin, PhD**[*,‡], **Camden Bay, PhD**[*,‡], **Stephan E. Maier, MD, PhD**[*,‡], **Adam S. Kibel, MD**[‡,‖], **Clare M. Tempany, MB, BCh**[*,‡], **Fiona M. Fenness, MB, BCh, PhD**[*,‡]

[*]Department of Radiology, Brigham and Women's Hospital, Boston, MA

[†]University Clinic Magdeburg, Otto von Guericke University, Magdeburg, Germany

[‡]Harvard Medical School, Boston, MA

[§]Clinical Sciences Lund, Lund University, Lund, Sweden

[‖]Department of Urology, Brigham and Women's Hospital, Boston, MA.

Abstract

Objectives: The objectives of this exploratory study were to investigate the feasibility of multidimensional diffusion magnetic resonance imaging (MddMRI) in assessing diffusion heterogeneity at both a macroscopic and microscopic level in prostate cancer (PCa).

Materials and Methods: Informed consent was obtained from 46 subjects who underwent 3.0-T prostate multiparametric MRI, complemented with a prototype spin echo–based MddMRI sequence in this institutional review board–approved study. Prostate cancer tumors and comparative normal tissue from each patient were contoured on both apparent diffusion coefficient and MddMRI-derived mean diffusivity (MD) maps (from which microscopic diffusion heterogeneity [MKi] and microscopic diffusion anisotropy were derived) using 3D Slicer. The discriminative ability of MddMRI-derived parameters to differentiate PCa from normal tissue was determined using the Friedman test. To determine if tumor diffusion heterogeneity is similar on macroscopic and microscopic scales, the linear association between SD of MD and mean MKi was estimated using robust regression (bisquare weighting). Hypothesis testing was 2 tailed; *P* values less than 0.05 were considered statistically significant.

Results: All MddMRI-derived parameters could distinguish tumor from normal tissue in the fixed-effects analysis ($P < 0.0001$). Tumor MKi was higher ($P < 0.05$) compared with normal tissue (median, 0.40; interquartile range, 0.29–0.52 vs 0.20–0.18; 0.25), as was tumor microscopic diffusion anisotropy (0.55; 0.36–0.81 vs 0.20–0.15; 0.28). The MKi could not be predicted (no significant association) by SD of MD. There was a significant correlation between tumor volume and SD of MD ($R^2 = 0.50$, slope = 0.008 μm^2/ms per millimeter, $P < 0.001$) but not between tumor volume and MKi.

Correspondence to: Fiona M. Fennessy, MB, BCh, PhD, Department of Radiology, Brigham and Women's Hospital, 75 Francis St, Boston, MA 02115. ffennessy@bwh.harvard.edu.

Conflicts of interest: For the remaining authors, no conflicts or sources of funding were declared.

Conclusions: This explorative study demonstrates that MddMRI provides novel information on MKi and microscopic anisotropy, which differ from measures at the macroscopic level. MddMRI has the potential to characterize tumor tissue heterogeneity at different spatial scales.

Keywords

multiparametric magnetic resonance imaging; prostate cancer; diffusion-weighted imaging; macroscopic diffusion heterogeneity; microscopic diffusion heterogeneity; anisotropy

Prostate cancer (PCa) is a heterogeneous cancer,[1] with intertumoral and intratumoral heterogeneity thought to be a major reason for variable clinical outcomes, even among patients with tumors of similar histologic type, stage, and grade.[2] Resultant challenges in risk prediction could potentially be addressed with a noninvasive method of characterizing heterogeneity.

Diffusion-weighted imaging (DWI) can discriminate indolent from clinically significant PCa.[3–5] The apparent diffusion coefficient (ADC) value, derived from DWI, has a negative correlation with pathology Gleason grade[6–10] and with tumor cellularity on pathology.[11] It is thought to be determined by water diffusion in luminal and ductal space[12,13] and cellular density.[14] Diffusivity parameters such as ADC or mean diffusivity (MD) derived from diffusion tensor imaging can probe tumor diffusion heterogeneity on a macroscopic level by comparing values across voxels. However, for any single voxel, these parameters capture the average rate of diffusion and are therefore insensitive to the diffusion heterogeneity within the individual voxel, that is, heterogeneity on the “microscopic” scale. There has been much interest of late in novel diffusion imaging sequences for assessment of PCa.[15,16] Microstructure magnetic resonance imaging (MRI) techniques that use biophysical models to estimate apparent cellular volume fractions have demonstrated improved differentiation of PCa from benign prostate tissue in comparison to standard ADC,[17,18] with early attempts to also incorporate diffusion time dependence and T2-dependence to characterize tumor.[19] Model-free approaches seek to create signal representations to probe diffusional kurtosis,[20] which can capture tissue heterogeneity on the subvoxel scale,[21,22] such that a mixture of dense and loose tissue will exhibit a mixture of slow and fast diffusivity, and high kurtosis. However, all examples of advanced diffusion encoding in prostate to date rely on diffusion encoding along a single direction per signal readout and therefore conflate the effects of variable diffusivity, microscopic diffusion anisotropy (MKa), and orientation dispersion.[23]

Multidimensional diffusion MRI (MddMRI),[23,24] unlike other advanced diffusion techniques, can measure MKa separate to other kinds of diffusional heterogeneity, none of which is possible with conventional diffusion encoding. Multidimensional diffusion MRI separates anisotropic and isotropic (MKa and microscopic diffusion heterogeneity [MKi]) contributions of diffusional kurtosis in a given voxel. Microscopic diffusion heterogeneity reflects the average microscopic variance of directional diffusion (diffusion anisotropy), and MKi reflects the average microscopic variance of directionally invariant diffusivities (isotropic diffusivities). Diffusion analysis with MddMRI has previously been deployed to characterize the microstructure of the brain.[25–27] However, the potential of MddMRI has yet to be explored in the context of PCa imaging. The current challenges in PCa imaging,

such as difficulty in finding sparse tumors interspersed between normal-appearing tissue[13,28] or indeed identification of aggressive cribriform-shaped cells,[29] underscore the need for measures of both microstructure anisotropy and heterogeneity to be investigated.

The primary goal of this exploratory study was to determine the feasibility of MddMRI in assessing prostate tissue diffusion heterogeneity and anisotropy at different spatial scales, both between voxels (macroscopic) and within voxels (microscopic), in a clinical population of patients suspected of having PCa. We explored how MKi and MKa varied across tumor, normal peripheral zone (nPZ), and normal transitional zone (nTZ), to determine if the addition of MKi and MKa provides novel information, which would motivate the future use of MddMRI in a larger clinical study.

MATERIALS AND METHODS

Patients

This prospective feasibility study was approved by the institutional review board and in compliance with the Health Insurance Portability and Accountability Act. Written informed consent was prospectively obtained from 55 men, who had a clinical suspicion of having PCa and were referred for prostate mpMRI examinations between July 2018 and September 2019.

MRI Data Acquisition

All MRIs were performed at 3 T (Prisma; Siemens Healthcare, Erlangen, Germany) using an 18-channel pelvic phased array coil[30] and supplemented with a prototype spin echo–based MddMRI sequence.[31] Conventional DWI protocol was acquired with the vendor-provided echo planar spin echo sequence in an axial plane with b-values of 50 and 1400 s/mm^2 along 6 independent directions. The following imaging parameters were used: TE (echo time) = 64 milliseconds, TR (repetition time) = 4800 milliseconds, FOV (field of view) = 219 × 112 mm^2, acquisition matrix = 90 × 46, in-plane resolution 2.4 × 2.4 mm^2, slice thickness = 4 mm without gap, averages = 1 (b = 50 s/mm^2) and 14 (b = 1400 s/mm^2), no in-plane acceleration, partial Fourier = 0.75, δ = 9.7 milliseconds, Δ = 19.1 milliseconds, and diffusion time = 15.9 milliseconds. The ADC and fractional anisotropy (FA) maps were calculated using the scanner software.[32]

Multidimensional diffusion MRI was used to acquire data in axial planes congruent with the DWI protocol. The pulse sequence uses gradient waveforms that encode diffusion along multiple directions with each signal preparation. Instead of describing the experiment with a single b-value and encoding direction, it is described with a b-tensor that can have full rank.[24] In this study, we used both linear and spherical b-tensors. The linear and spherical variants are used to yield maximal and minimal sensitivity to MKa, respectively. By comparing the linear and spherical b-tensors in a statistical kurtosis signal representation, we measured diffusion non-Gaussianity caused by MKa and isotropic diffusion heterogeneity (MKi).[23,33] The following imaging parameters were used: TE = 75 milliseconds, TR = 2400 milliseconds, FOV = 260 × 260 mm^2, acquisition matrix = 130 × 130, in-plane resolution 2 × 2 mm^2, slice thickness = 4 mm without gap, partial Fourier = 6/8, and

in-plane acceleration factor 2 (generalized autocalibrating partially parallel acquisition). We used b-values of 200, 500, 800, 1100, and 1400 s/mm^2 in 8, 8, 12, 10, and 12 independent directions (linear b-tensor encoding) and 200, 500, 800, and 1100 s/mm^2 repeated 6, 6, 8, and 10 times (spherical b-tensor encoding), respectively. Waveforms for spherical encoding were optimized numerically and compensated for concomitant gradient effects.[34,35] To achieve minimal TE, the waveforms were not matched with respect to their diffusion time spectra,[36] and a single diffusion time that holds for all encodings cannot be formulated. The total scan time for MddMRI was less than 4 minutes.

Before model fitting, the data were smoothed in-plane with a Gaussian filter with a standard deviation of 1.2 mm. Motion correction was not applied. The signal representation described by Westin et al[24] was used to calculate the MD, MKa, and MKi, according to the implementation of the multidimensional diffusion framework.[24] The sum of MKi and MKa, which is similar to the mean kurtosis of DKI,[33] was also computed.

Image Analysis

All regions of interest (ROIs) were volumetrically annotated and analyzed using 3D Slicer[37] by a radiologist with 18 years of experience in GU imaging (FMF). For each case, the reader confirmed its diagnostic quality before contouring. Prostate pathology reports were available to the radiologist at the time of image analysis. Prostate cancer foci were pathology confirmed with either transrectal ultrasound–guided prostate biopsy, with MR-US–guided fusion biopsy and/or with radical prostatectomy. Both ADC maps (b1400) and MddMRI-derived MD maps for tumor ROIs (when present) were annotated, as previously described.[38] The tumor ROIs were identified based upon both a PI-RADS v2.1 assessment score of either 4 or 5[30] (indicating that clinically significant cancer was likely present) and pathological proof of PCa per review of the electronic medical records. In all cases of diagnostic quality, normal-appearing ROIs (normal ROIs) were placed on both PZ and TZ areas without evidence of tumor, on the side contralateral to the tumor ROI but on the same or adjacent axial slice.[38] The ADC metrics were obtained from ADC map contours, and the MddMRI parameters (MD, MKa, MKi, and MD) were extracted from MD map contours. Figure 1 demonstrates a typical segmentation of tumor ROI and normal ROI in the prostate.

Two cases underwent detailed exploratory MRI correlation with corresponding hematoxylin-eosin–stained pathology tissue sections. In these 2 cases, FA was also obtained from the MD contour, as a measure of anisotropy at the voxel level.

Correlative Clinical and Pathological Data Extraction

Prostate gland volumes[39] were obtained from the MR prostate report. The following data were obtained from the EMR: age, serum prostate-specific antigen (PSA), clinical stage, pathology confirmation of PCa, method of pathology confirmation (biopsy and/or prostatectomy), and highest Gleason score. The PSA density was calculated using prostate volume and PSA serum level closest to the date of the mpMRI.

Statistical Analysis

Patient demographics were compared between those with and without tumor using Wilcoxon rank sum tests. Correlation between mean ADC and mean MD for both normal ROIs and tumor ROIs was assessed with Spearman rank correlation. Prostate diffusion heterogeneity on a macroscopic scale (mean and SD of MD) and on a microscopic scale (isotropic diffusion heterogeneity mean MKi) and microscopic tissue anisotropy (mean MKa) were compared between the tumor ROIs and normal ROIs. Comparisons were performed in patients with pathology-proven tumors using the Friedman test to account for multiple measurements per patient (ie, tumor, nPZ, and nTZ measurement). Receiver operating characteristic (ROC) curves were generated to visualize how mean ADC and mean MddMRI metrics performed in the differentiation of tumor ROI and normal ROI.

To determine if tumor MKi reflects the same information as diffusion heterogeneity on a macroscopic scale, the linear association was estimated between SD of MD and mean MKi using robust regression (bisquare weighting). Tumor ROIs were divided by their median volume into 2 groups and analyzed separately to account for tumor ROI volume as a potential confounder of diffusion heterogeneity. Due to the larger volume of normal ROIs, Spearman rank correlation was used to obtain a correlation coefficient between SD of MD and the mean of MKi for nPZ and nTZ. Analyses were performed using R (version 3.6.1), SAS 9.4 (SAS Institute Inc, Cary, NC), and Matlab version 9.6.0.1214997 (R2019a). Hypothesis testing was 2 tailed, and *P* values less than 0.05 were considered statistically significant. Summary statistics were used to describe the demographic and imaging characteristics of the sample.

RESULTS

Informed consent was obtained in 55 patients, and MddMRI acquisition was feasible in all cases. Nine cases were excluded from the final analysis due to prior PCa treatment (n = 6) or failure to complete the full MR examination (n = 3). Patient flowchart is provided in Figure 2. Thus, 46 patients were included in this analysis (mean age, 67 ± 7 years). The median PSA level was 5.68 ng/mL (interquartile range [IQR], 4.33–8.08), and the median PSA density was 0.10 ng/mL^2 (IQR, 0.08–0.16), with no significant difference between those with PCa compared with those without PCa. The median prostate gland volume was 55 mL (IQR, 37.3–72), with a higher volume in those without PCa (62.0 mL; IQR, 45.20–88.0) compared with those with PCa (45.0 mL; IQR, 35.10–66.0) ($P = 0.018$). Patient demographic data are provided in Table 1. Prostate cancer was pathologically proven in 50% (n = 23) of patients, all of whom had tumor ROIs identified and contoured. A total of 6 tumors were in the TZ and 17 in the PZ. Tumor was pathologically confirmed through MR-US fusion biopsy in 74% (n = 17) and transrectal ultrasound–guided systematic biopsy in 26% (n = 6) of patients. Eight patients underwent radical prostatectomy with whole gland pathology analysis. The mean time between the prostate biopsy and MddMRI was 3.4 ± 2.5 months. The median MddMRI-based tumor volume was 256 mm^3. An illustrative example of contoured MddMRI-derived metrics and ADC in a pathologically proven Gleason score 4 + 3 tumor is demonstrated in Figure 3.

The mean ADC and MddMRI-derived MD showed a moderate to strong correlation, as outlined in Figure 4. Spearman rank correlations (ρ_S) between ADC and MD were as follows: tumor ROI (ρ_S = 0.89; 95% confidence interval [CI], 0.80–0.96; $P < 0.0001$); normal ROI nTZ (ρ_S = 0.63; 95% CI, 0.41–0.78; $P < 0.0001$); and normal ROI nPZ (ρ_S = 0.59; 95% CI, 0.35–0.75; $P < 0.0001$).

The Friedman test provided evidence that median MD significantly decreased sequentially from nPZ (1.78 μm^2/ms) to nTZ (1.38 μm^2/ms) to tumor (1.07 μm^2/ms) ($P < 0.0001$). In contrast, median MKa and MKi increased from nPZ to nTZ to tumor as follows: MKa (0.20 [nPZ], 0.37 [nTZ], 0.55 [tumor], $P < 0.0001$) and MKi (0.20 [nPZ], 0.32 [nTZ], 0.40 [tumor], $P = 0.0001$). All MddMRI-derived parameters (mean MD, mean MKi, and mean MKa) could distinguish tumor ROIs from normal ROIs with a statistically significant difference ($P < 0.0001$) (see Table 2). The area under the curve (AUC) ROC analyses for differentiating tumor ROI from normal ROI were as follows: ADC was 0.95; MD, 0.96; MKa and MKi combined, 0.90, as outlined in Figure 5. The AUC ROC analyses for differentiating nonclinically significant PCa (ie, Gleason score of 6) from clinically significant PCa (ie, Gleason score of 7 or more) were as follows: ADC, 0.66; MD, 0.63; MKa and MKi combined, 0.62, as outlined in Figure 6.

Microscopic diffusion heterogeneity could not be predicted by macroscopic diffusion heterogeneity (SD of MD): there was no correlation between mean MKi and SD of MD (ρ_S = 0.10; 95% CI, −0.34 to 0.50; $P = 0.67$) within tumor nor within normal prostate tissue (nPZ: ρ_S = 0.01; 95% CI, 0.28–0.30; $P = 0.96$; nTZ: ρ_S = 0.05; 95% CI, 0.24–0.35; P = 0.74).

There was a significant correlation between tumor volume and macroscopic heterogeneity (R^2 = 0.50, slope = 0.008 μm^2/ms per millimeter; $P < 0.001$) (see Fig. 7), but no significant correlation between tumor volume and MKi. To determine if smaller tumor ROI volumes could be potential confounders of diffusion heterogeneity, tumor ROIs were dichotomized tumors based on median volume (smaller, <256 mm^3, n = 12 and larger, >256 mm^3, n = 11), but no significant linear correlation was found (see Fig. 7).

Although detailed pathological correlation for all cases with tumor is outside the scope of this exploratory study, Figure 8 is a pictorial example of 2 patients with tumors of the same grade with relatively similar MKi but markedly different FA (indicative of different levels of macroscopic and microscopic anisotropy), and how hematoxylin-eosin from prostatectomy specimens may help explain our findings.

DISCUSSION

In this exploratory study, we show that MddMRI is technically feasible in men suspected of having PCa, and that it has the potential to provide several novel imaging parameters for in-depth assessment of both macroscopic and microscopic PCa heterogeneity. We demonstrate that macroscopic and microscopic diffusivity parameters vary across normal tissue and within areas of the tumor. As with prior studies, mean ADC and MD are decreased within areas of tumor, but this study uniquely demonstrates that MKi and microscopic tissue

anisotropy increase from nPZ to nTZ to tumor. In addition, MKi could not be predicted by macroscopic diffusion heterogeneity. This exploratory study therefore provides motivation to study MddMRI in a future, larger clinical study.

As expected, the positive correlation between ADC and MD is reflective of the fact that both measurements are influenced by tissue density within the voxel.[11] Although both reflect diffusion on a macroscopic level, the observed differences may be explained by the fact that the measurements are derived from different imaging protocols, different signal representations, and different postprocessing methods. A potential advantage of using MD is that it captures a quantity that correlates with ADC, but due to the different signal representation, it is free of bias from non-Gaussian diffusion and b-value dependence.[20]

Another validation of metrics derived from MddMRI is the sum of MKi and MKa, which are expected to represent established kurtosis metrics,[20] and indeed in our study, we found the summation of MKi and MKa values to be similar to previously reported diffusion kurtosis in earlier prostate diffusion imaging studies.[40,41]

This study shows that MKi and MKa increase from nPZ to nTZ to tumor. Although these findings require further validation in larger numbers with detailed histology correlation, they are likely related to an increase in within-voxel diffusion heterogeneity from nPZ to nTZ to tumor and may be reflective of the differences in relative compartment volumes of epithelium, stroma, and ductal space between normal PZ and TZ and tumor.[42]

A possible limitation of subvoxel metrics is that similar features manifest on the macroscopic scale and therefore offset the need for more advanced imaging methods to measure them. Therefore, we tested if macroscopic and microscopic variances in diffusivity were correlated but found no evidence for such. Therefore, it is likely that the macroscales and microscales may indeed reflect different structural features of prostate tissue, suggesting that both be further explored.

The absence of correlation between macroscopic diffusion heterogeneity (SD of MD) and MKi implies that tissue heterogeneity at the scale of voxels is independent of microscopic tissue heterogeneity, which is novel. Elevation of either measure may be associated with an unfavorable clinical outcome, but such association must be confirmed in future studies. As tumor volumes varied, we investigated whether tumor ROI size could be a cofounder of microscopic or macroscopic heterogeneity. With increasing tumor size, macroscopic diffusion heterogeneity increases, but microscopic heterogeneity does not. Moreover, we found that tumor size may confound the interpretation of macroscopic heterogeneity.

Monoexponential ADC is considered standard of care for assessment of patients who have a clinical suspicion of having PCa and is an established predictive biomarker for PCa.[7,8,28,38] The ROC analysis in differentiating tumor from normal tissue found AUC values similar to those published previously for ADC,[43] validating our measurements. It is difficult to improve on an AUC of 95% in differentiation of tumor and benign tissue, and indeed the combined MddMRI parameters MKa + MKi do not improve on the differentiation (AUC 90%). However, the goal of this exploratory study was not to improve upon the differentiation of cancer from benign tissue, but rather to determine if MddMRI is capable

of providing new quantitative information related to both macroscopic and microscopic diffusion heterogeneity.

The clinical interpretations of the novel microstructural imaging biomarkers MKi and MKa are as yet unknown and will require a detailed correlative histopathology.[44,45] However, the theoretical benefit of MddMRI is that it can distinguish between non-Gaussianity caused by MKa and the presence of multiple isotropic diffusivities (MKi) on the subvoxel scale. These parameters have been previously linked to anisotropic cell structures and variable cell density by quantitative histology in intracranial tumors,[33] features that may provide valuable biomarkers but are beyond the reach of conventional quantitative diffusion imaging methods.[36] An ability of MddMRI to assess PCa heterogeneity and anisotropy on a microscopic level offers possibilities for further exploration of prostate tumor microstructure, including detection of sparse tumor and assessment of tumor cell type, which are challenges with current prostate MRI.

This study has several limitations. First, only half of our patient population had a pathological PCa diagnosis, and many of these tumors were small, limiting our correlative analysis. The number of tumors in the transitional zone was small, preventing comparison with peripheral zone tumors, although this was not the goal of this exploratory study. Furthermore, the ROIs were independently defined on ADC and MD maps, and although visually confirmed to be in the same anatomical location, there is risk of incomplete overlap. Another limitation is that the value and meaning of MddMRI parameters in the prostate will need to be validated in a larger patient population with detailed histopathology correlation. Further studies are necessary to consider the effects of relaxation, exchange, diffusion time, and microscopic kurtosis to avoid confounding factors in the analysis.[36,46] Indeed, if the multi-Gaussian approximation is violated, the waveforms used herein may interact with the tissue geometry and manifest as a parameter bias.[47] Finally, parameter averages and standard deviations are sensitive to partial volume effects and therefore depend on spatial resolution. Using larger voxels increases the risk of conflating heterogeneous diffusion on the microscopic scale with partial volume effects.

In conclusion, this exploratory study demonstrates that MddMRI is feasible and valid for assessing prostate tissue diffusion heterogeneity on both macroscopic and microscopic scales and can also provide an estimate of MKa in a clinical population of patients suspected of having PCa. We found no evidence that macroscopic and microscopic diffusion heterogeneity reflect the same tissue features, indicating that these are independent quantities. Considering the interpatient and intrapatient heterogeneous nature of PCa and armed with the knowledge that studies in other tumor types have demonstrated a role for multidimensional microstructure imaging in cancer diagnosis,[48] a role for MddMRI in PCa looks very promising, prompting further investigation of advanced microscopic imaging techniques for PCa assessment.

Acknowledgments

sources of funding: F.M.F., C.M.T., and S.E.M. are funded through NIH P41EB 015898, NIH P41EB 028741, and NIH R01CA241817. F.S. and C.-F.W. are funded through NIH P41EB 015902.

REFERENCES

1. Tolkach Y, Kristiansen G. The heterogeneity of prostate cancer: a practical approach. Pathobiology. 2018;85:108–116. [PubMed: 29393241]
2. Liu W, Xie CC, Thomas CY, et al. Genetic markers associated with early cancer-specific mortality following prostatectomy. Cancer. 2013;119:2405–2412. [PubMed: 23609948]
3. Vos EK, Kobus T, Litjens GJS, et al. Multiparametric magnetic resonance imaging for discriminating low-grade from high-grade prostate cancer. Invest Radiol. 2015;50:490–497. [PubMed: 25867656]
4. Vargas HA, Akin O, Franiel T, et al. Diffusion-weighted endorectal MR imaging at 3 T for prostate cancer: tumor detection and assessment of aggressiveness. Radiology. 2011;259:775–784. [PubMed: 21436085]
5. Itou Y, Nakanishi K, Narumi Y, et al. Clinical utility of apparent diffusion coefficient (ADC) values in patients with prostate cancer: can ADC values contribute to assess the aggressiveness of prostate cancer? J Magn Reson Imaging. 2011;33: 167–172. [PubMed: 21182135]
6. Rosenkrantz AB, Triolo MJ, Melamed J, et al. Whole-lesion apparent diffusion coefficient metrics as a marker of percentage Gleason 4 component within Gleason 7 prostate cancer at radical prostatectomy. J Magn Reson Imaging. 2014;41:708–714. [PubMed: 24616064]
7. Hassanzadeh E, Alessandrino F, Olubiyi OI, et al. Comparison of quantitative apparent diffusion coefficient parameters with prostate imaging reporting and data system V2 assessment for detection of clinically significant peripheral zone prostate cancer. Abdom Radiol (NY). 2018;43:1237–1244. [PubMed: 28840280]
8. Alessandrino F, Taghipour M, Hassanzadeh E, et al. Predictive role of PI-RADSv2 and ADC parameters in differentiating Gleason pattern 3 + 4 and 4 + 3 prostate cancer. Abdom Radiol (NY). 2019;44:279–285. [PubMed: 30066169]
9. Cobelli FD, Taghipour M, Hassanzadeh E, et al. Apparent diffusion coefficient value and ratio as noninvasive potential biomarkers to predict prostate cancer grading: comparison with prostate biopsy and radical prostatectomy specimen. Am J Roentgenol. 2015;204:550–557. [PubMed: 25714284]
10. Woo S, Kim SY, Cho JY, et al. Preoperative evaluation of prostate cancer aggressiveness: using ADC and ADC ratio in determining Gleason score. AJR Am J Roentgenol. 2016;207:114–120. [PubMed: 27077643]
11. Chen L, Liu M, Bao J, et al. The correlation between apparent diffusion coefficient and tumor cellularity in patients: a meta-analysis. PLoS One. 2013;8:e79008.
12. Selnæs KM, Vettukattil R, Bertilsson H, et al. Tissue microstructure is linked to MRI parameters and metabolite levels in prostate cancer. Front Oncol. 2016;6:146. [PubMed: 27379208]
13. Langer DL, van der Kwast TH, Evans AJ, et al. Intermixed normal tissue within prostate cancer: effect on MR imaging measurements of apparent diffusion coefficient and T2—sparse versus dense cancers. Radiology. 2008;249:900–908. [PubMed: 19011187]
14. Gibbs P, Liney GP, Pickles MD, et al. Correlation of ADC and T2 measurements with cell density in prostate cancer at 3.0 Tesla. Invest Radiol. 2009;44:572–576. [PubMed: 19692841]
15. Lemberskiy G, Rosenkrantz AB, Veraart J, et al. Time-dependent diffusion in prostate cancer. Invest Radiol. 2017;52:405–411. [PubMed: 28187006]
16. Aksit Ciris P, Chiou J-YG, Glazer DI, et al. Accelerated segmented diffusion-weighted prostate imaging for higher resolution, higher geometric fidelity, and multi-b perfusion estimation. Invest Radiol. 2019;54:238–246. [PubMed: 30601292]
17. Johnston EW, Bonet-Carne E, Ferizi U, et al. VERDICT MRI for prostate cancer: intracellular volume fraction versus apparent diffusion coefficient. Radiology. 2019;291:391–397. [PubMed: 30938627]
18. Panagiotaki E, Chan RW, Dikaios N, et al. Microstructural characterization of normal and malignant human prostate tissue with vascular, extracellular, and restricted diffusion for cytometry in tumours magnetic resonance imaging. Invest Radiol. 2015;50:218–227. [PubMed: 25426656]

19. Chatterjee A, Bourne RM, Wang S, et al. Diagnosis of prostate cancer with noninvasive estimation of prostate tissue composition by using hybrid multidimensional MR imaging: a feasibility study. Radiology. 2018;287:864–873. [PubMed: 29393821]
20. Jensen JH, Helpern JA, Ramani A, et al. Diffusional kurtosis imaging: the quantification of non-Gaussian water diffusion by means of magnetic resonance imaging. Magn Reson Med. 2005;53:1432–1440. [PubMed: 15906300]
21. Cheung MM, Hui ES, Chan KC, et al. Does diffusion kurtosis imaging lead to better neural tissue characterization? A rodent brain maturation study. Neuroimage. 2009;45:386–392. [PubMed: 19150655]
22. Van Cauter S, Veraart J, Sijbers J, et al. Gliomas: diffusion kurtosis MR imaging in grading. Radiology. 2012;263:492–501. [PubMed: 22403168]
23. Eriksson S, Lasic S, Topgaard D. Isotropic diffusion weighting in PGSE NMR by magic-angle spinning of the q-vector. J Magn Reson. 2013;226:13–18. [PubMed: 23178533]
24. Westin C-F, Knutsson H, Pasternak O, et al. Q-space trajectory imaging for multidimensional diffusion MRI of the human brain. Neuroimage. 2016;135:345–362. [PubMed: 26923372]
25. Lampinen B, Szczepankiewicz F, Mårtensson J, et al. Towards unconstrained compartment modeling in white matter using diffusion-relaxation MRI with tensor-valued diffusion encoding. Magn Reson Med. 2020;84:1605–1623. [PubMed: 32141131]
26. Tax CMW, Szczepankiewicz F, Nilsson M, et al. The dot-compartment revealed? Diffusion MRI with ultra-strong gradients and spherical tensor encoding in the living human brain. Neuroimage. 2020;210:116534.
27. Nilsson M, Szczepankiewicz F, Brabec J, et al. Tensor-valued diffusion MRI in under 3 minutes: an initial survey of microscopic anisotropy and tissue heterogeneity in intracranial tumors. Magn Reson Med. 2020;83:608–620. [PubMed: 31517401]
28. Glazer DI, Hassanzadeh E, Fedorov A, et al. Diffusion-weighted endorectal MR imaging at 3T for prostate cancer: correlation with tumor cell density and percentage Gleason pattern on whole mount pathology. Abdom Radiol (NY). 2017;42:918–925. [PubMed: 27770164]
29. Greenland NY, Cowan JE, Zhang L, et al. Expansile cribriform Gleason pattern 4 has histopathologic and molecular features of aggressiveness and greater risk of biochemical failure compared to glomerulation Gleason pattern 4. Prostate. 2020;80:653–659. [PubMed: 32220141]
30. Weinreb JC, Barentsz JO, Choyke PL, et al. PI-RADS Prostate Imaging - Reporting and Data System: 2015, version 2. Eur Urol. 2016;69:16–40. [PubMed: 26427566]
31. Szczepankiewicz F, Sjölund J, Ståhlberg F, et al. Tensor-valued diffusion encoding for diffusional variance decomposition (DIVIDE): technical feasibility in clinical MRI systems. PLoS One. 2019;14:e0214238.
32. Basser PJ, Mattiello J, LeBihan D. MR diffusion tensor spectroscopy and imaging. Biophys J. 1994;66:259–267. [PubMed: 8130344]
33. Szczepankiewicz F, van Westen D, Englund E, et al. The link between diffusion MRI and tumor heterogeneity: mapping cell eccentricity and density by diffusional variance decomposition (DIVIDE). Neuroimage. 2016;142:522–532. [PubMed: 27450666]
34. Sjölund J, Szczepankiewicz F, Nilsson M, et al. Constrained optimization of gradient waveforms for generalized diffusion encoding. J Magn Reson. 2015;261: 157–168. [PubMed: 26583528]
35. Szczepankiewicz F, Westin C, Nilsson M. Maxwell-compensated design of asymmetric gradient waveforms for tensor-valued diffusion encoding. Magn Reson Med. 2019;82:1424–1437. [PubMed: 31148245]
36. Szczepankiewicz F, Westin CF, Nilsson M. Gradient waveform design for tensor-valued encoding in diffusion MRI. J Neurosci Methods. 2021;348:109007.
37. Fedorov A, Beichel R, Kalpathy-Cramer J, et al. 3D slicer as an image computing platform for the quantitative imaging network. Magn Reson Imaging. 2012;30: 1323–1341. [PubMed: 22770690]
38. Fedorov A, Vangel MG, Tempany CM, et al. Multiparametric magnetic resonance imaging of the prostate: repeatability of volume and apparent diffusion coefficient quantification. Invest Radiol. 2017;52:538–546. [PubMed: 28463931]
39. Hricak H, Jeffrey RB, Dooms GC, et al. Evaluation of prostate size: a comparison of ultrasound and magnetic resonance imaging. Urol Radiol. 1987;9:1–8. [PubMed: 2440168]

40. Langkilde F, Kobus T, Fedorov A, et al. Evaluation of fitting models for prostate tissue characterization using extended-range b-factor diffusion-weighted imaging. Magn Reson Med. 2018;79:2346–2358. [PubMed: 28718517]

41. Suo S, Chen X, Wu L, et al. Non-Gaussian water diffusion kurtosis imaging of prostate cancer. Magn Reson Imaging. 2014;32:421–427. [PubMed: 24602826]

42. Bourne RM, Kurniawan N, Cowin G, et al. Microscopic diffusivity compartmentation in formalin-fixed prostate tissue. Magn Reson Med. 2012;68:614–620. [PubMed: 22807067]

43. Wang X, Hielscher T, Radtke JP, et al. Comparison of single-scanner single-protocol quantitative ADC measurements to ADC ratios to detect clinically significant prostate cancer. Eur J Radiol. 2021;136:109538.

44. Fennessy FM, Fedorov A, Penzkofer T, et al. Quantitative pharmacokinetic analysis of prostate cancer DCE-MRI at 3T: comparison of two arterial input functions on cancer detection with digitized whole mount histopathological validation. Magn Reson Imaging. 2015;33:886–894. [PubMed: 25683515]

45. Trivedi H, Turkbey B, Rastinehad AR, et al. Use of patient-specific MRI-based prostate mold for validation of multiparametric MRI in localization of prostate cancer. Urology. 2012;79:233–239. [PubMed: 22202553]

46. Henriques RN, Jespersen SN, Shemesh N. Correlation tensor magnetic resonance imaging. Neuroimage. 2020;211:116605.

47. Jespersen SN, Olesen JL, Ianuş A, et al. Effects of nongaussian diffusion on ‘isotropic diffusion’ measurements: an ex-vivo microimaging and simulation study. J Magn Reson. 2019;300:84–94. [PubMed: 30711786]

48. Turkbey B, Rosenkrantz AB, Haider MA, et al. Prostate Imaging Reporting and Data System Version 2.1: 2019 Update of prostate imaging Reporting and data system version 2. EurUrol. 2019;76:340–351.doi:10.1016/j.eururo.2019.02.033.

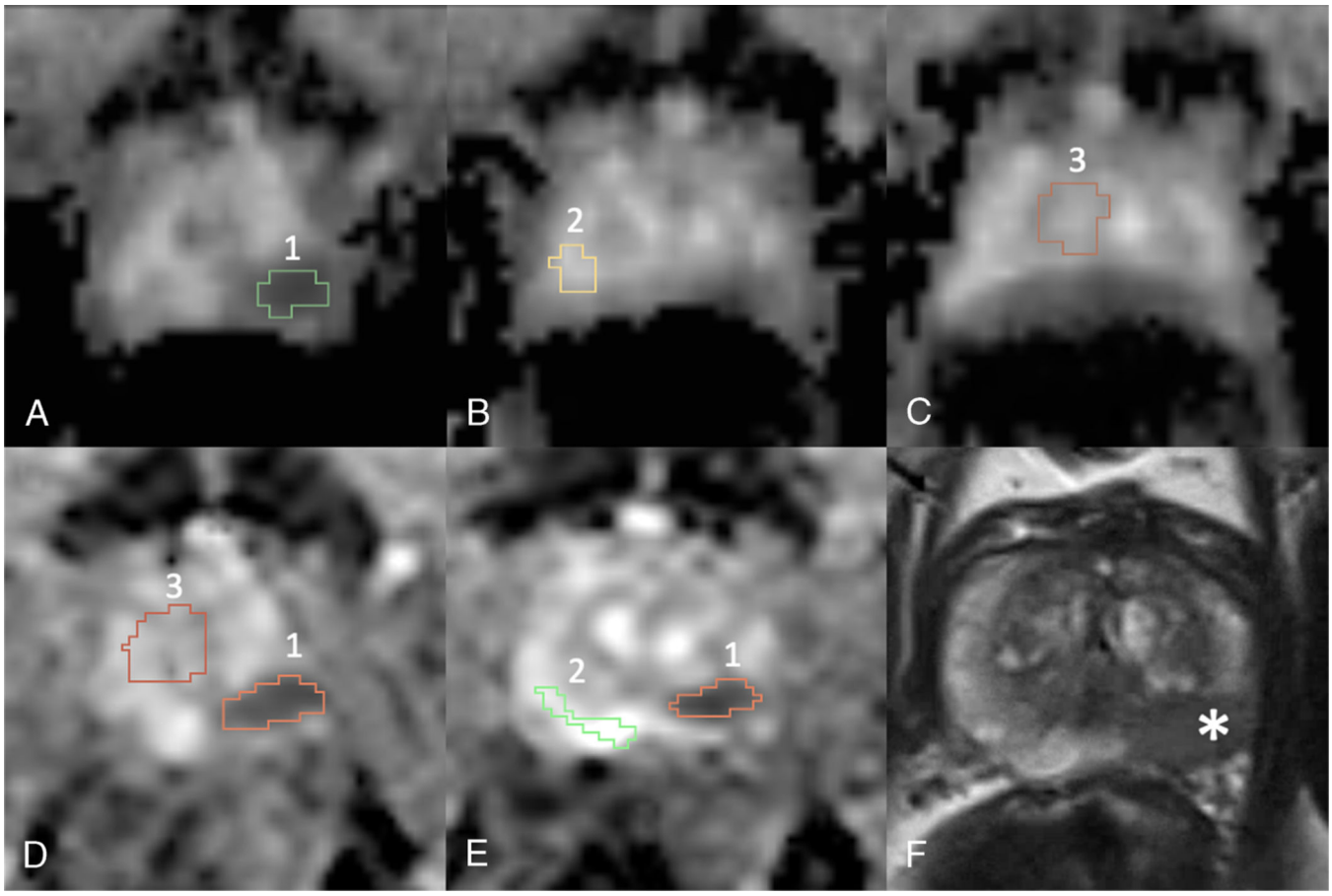

FIGURE 1.

Example of prostate segmentation on MRI of tumor (1), nPZ (2), and nTZ (3) using 3D Slicer in a 67-year-old man. Radical prostatectomy 5 months post-mpMRI examination revealed Gleason grade group 3 (Gleason score 4 + 3 = 7), with 60% Gleason pattern 4. Top row (A–C) shows axial MD map slices through different axial levels, and bottom row (D and E) shows different axial slices through ADC maps. Image F is a T2-weighted image at the same axial level as image D, with the tumor lesion indicated by an asterisk.

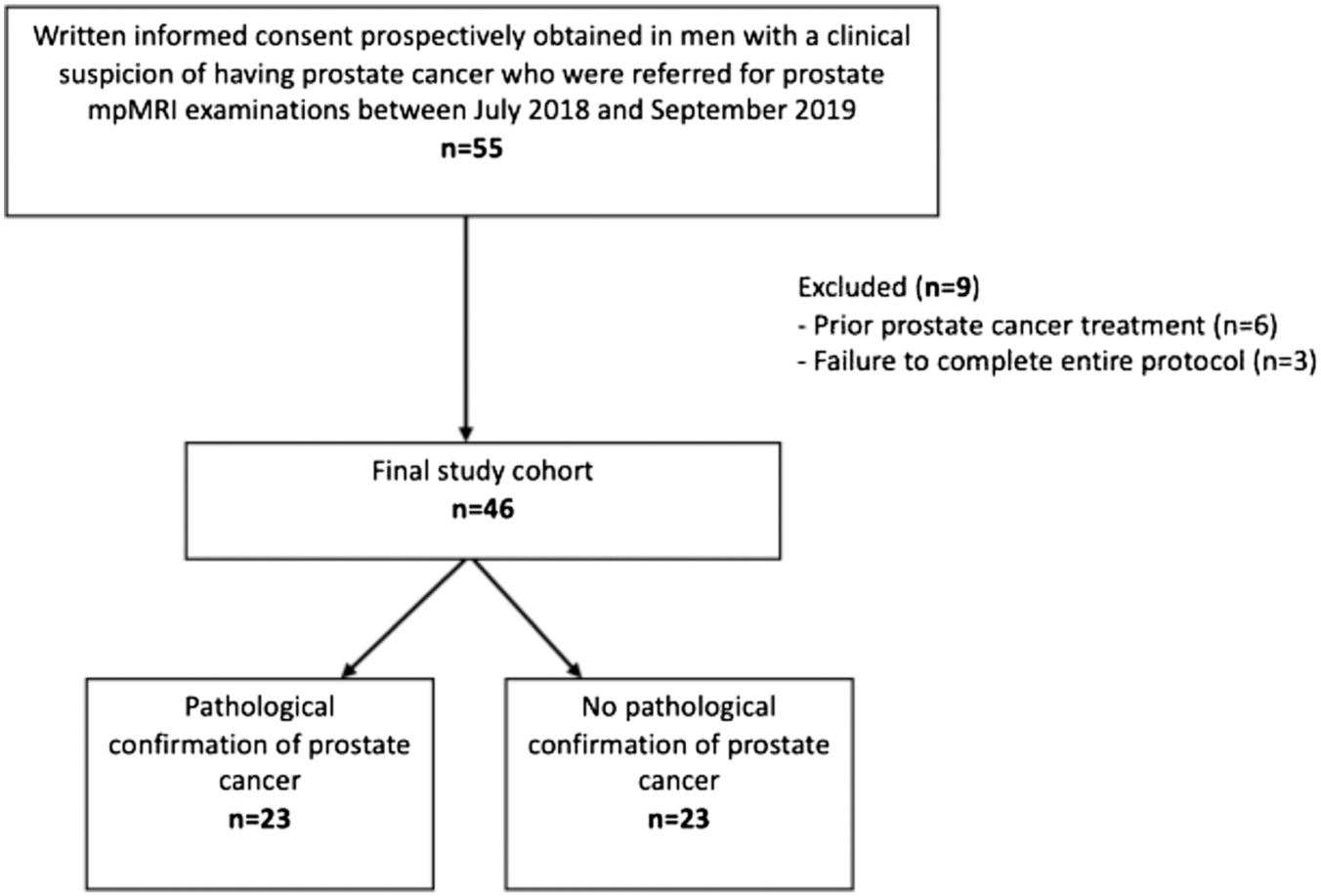

FIGURE 2.

Flowchart outlining the total patient number in whom informed consent for study participation was obtained, number of patients excluded and reason for exclusion from the study, and number of patients in whom a pathological diagnosis of prostate cancer was made.

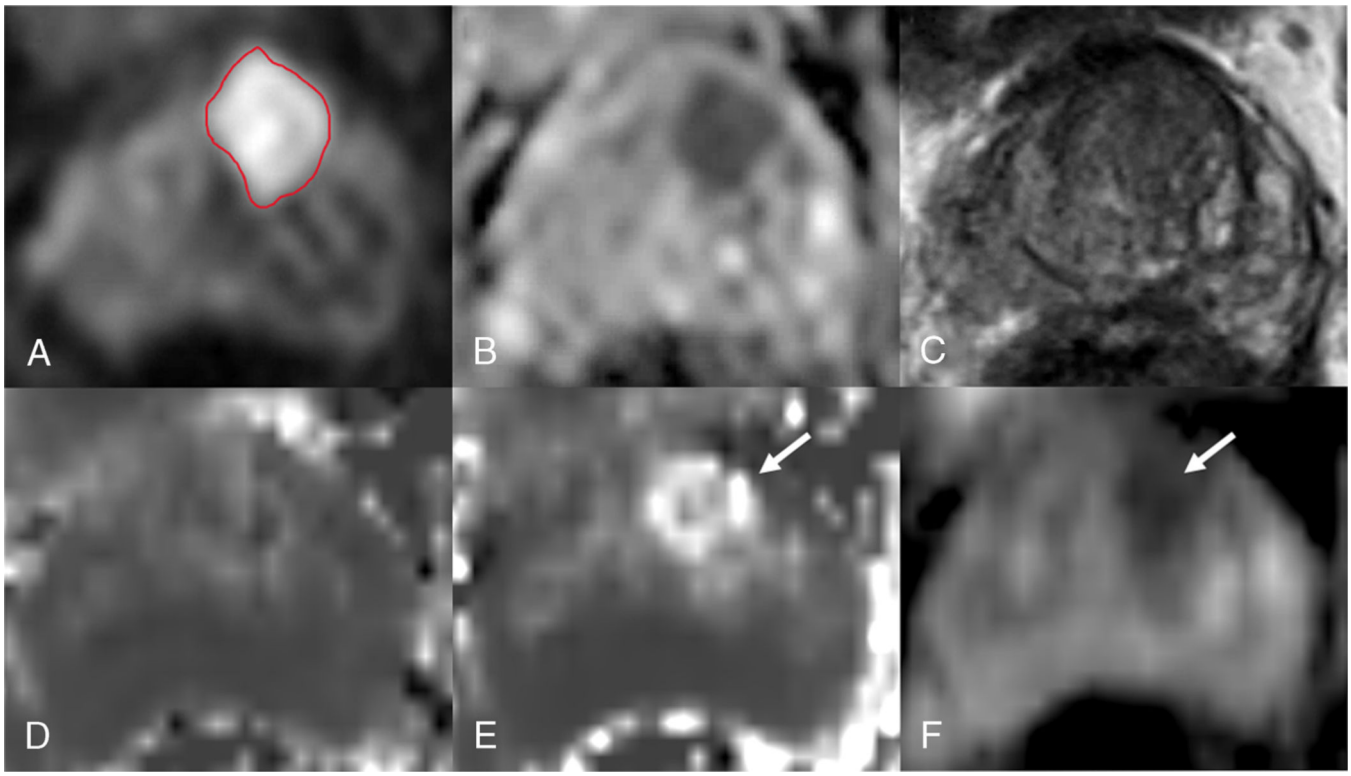

FIGURE 3.

Prostate MRI in a 66-year-old man with confirmed Gleason grade group 2 (Gleason score 3 + 4) on transrectal ultrasound–guided biopsy. Top row: (A) DWI (b = 1400 s/mm^2), (B) ADC map, (C) T2-weighted image; and bottom row: (D) MKa, (E) MKi, and (F) MD, through the same axial slice. These maps show a well-defined focal lesion in the left anterior prostate (contoured on 3D Slicer on image A) demonstrating high signal on A, restricted diffusion on B, and is ill-defined on T2 weighted images (C). Likewise, there is diffuse low signal on F, but heterogeneous increased microscopic tissue diffusion heterogeneity (E) and, to a lesser degree, slightly increased microscopic tissue anisotropy (D). This is an example of how measures of macroscopic and microscopic diffusion heterogeneity appear grossly dissimilar, with the addition of microscopic diffusion heterogeneity likely providing novel information.

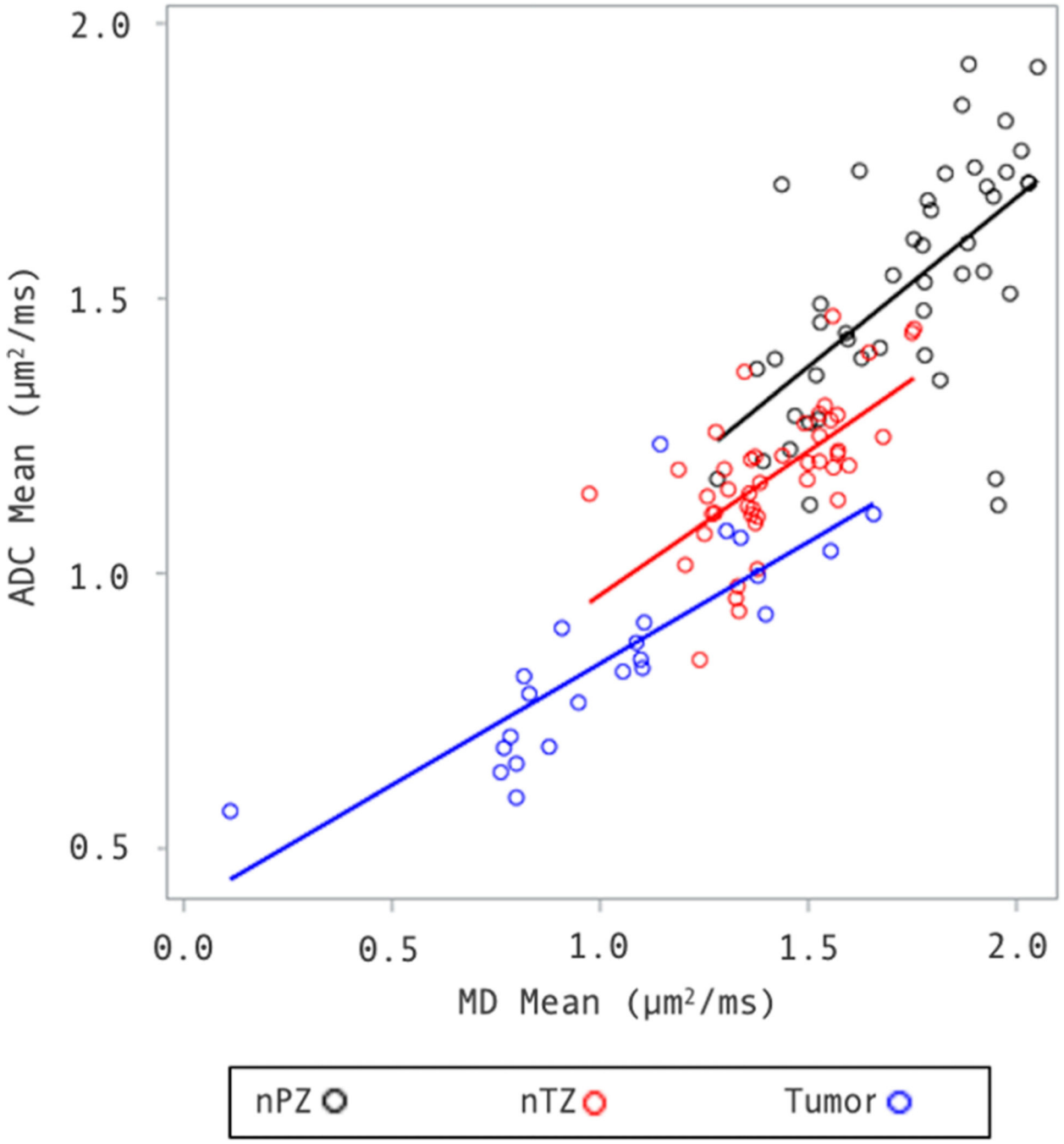

FIGURE 4.

Graphs show correlation between ADC (μm^2/ms) and MD (μm^2/ms) for tumor (ρ_s, 0.89; CI, 0.80–0.96), nPZ (ρ_s, 0.59; CI, 0.35–0.75), and nTZ (ρ_s, 0.63; CI, 0.41–0.78) (all *P*'s < 0.0001). Lines are lines of best fit.

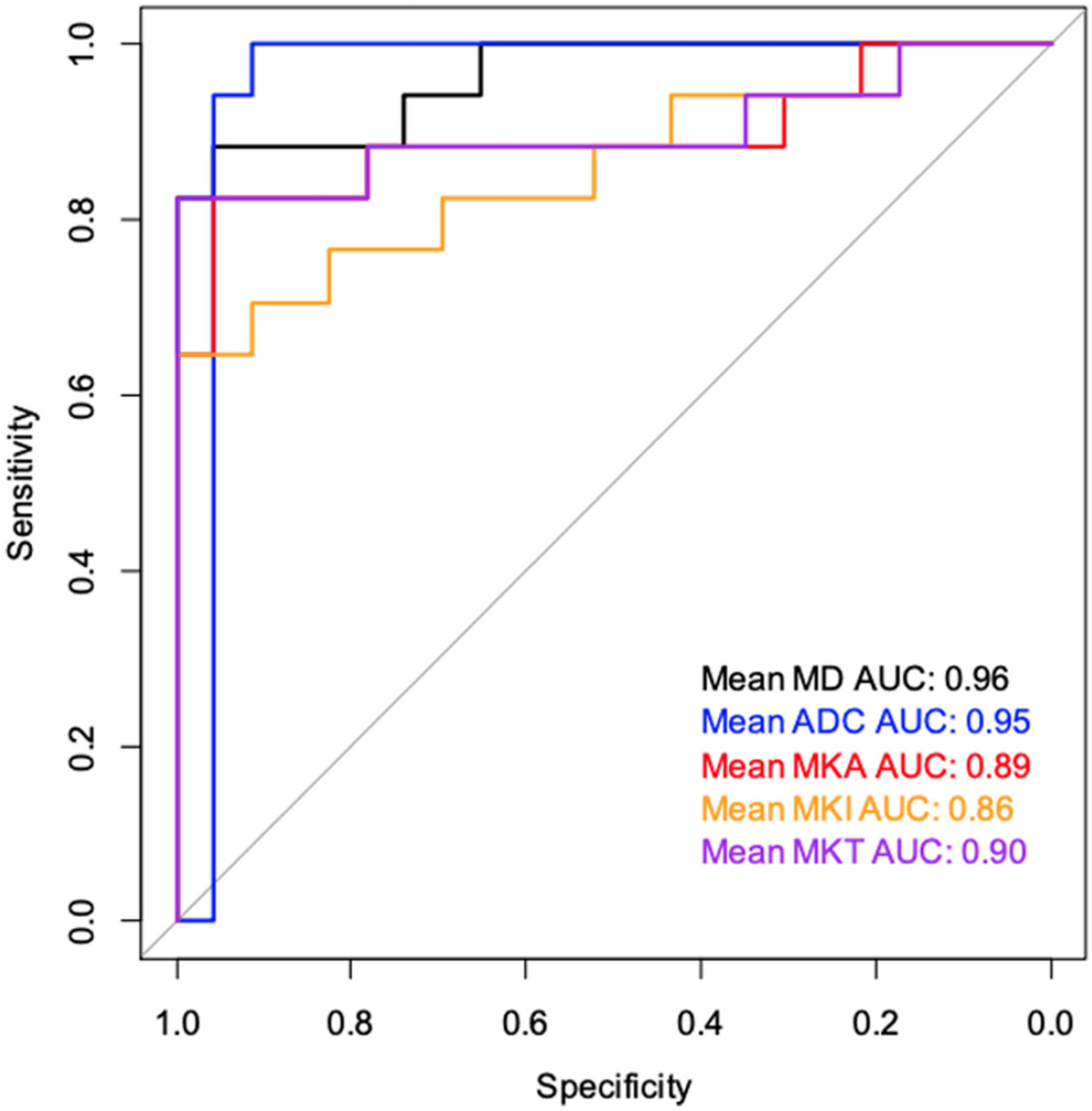

FIGURE 5.
ROC analysis using AUC for both ADC and MddMRI parameters (MD, MKa, MKi) in differentiating tumor ROI versus normal ROI. ROC indicates receiver operating characteristic curve; AUC, area under the curve; and ROI, tumor region of interest.

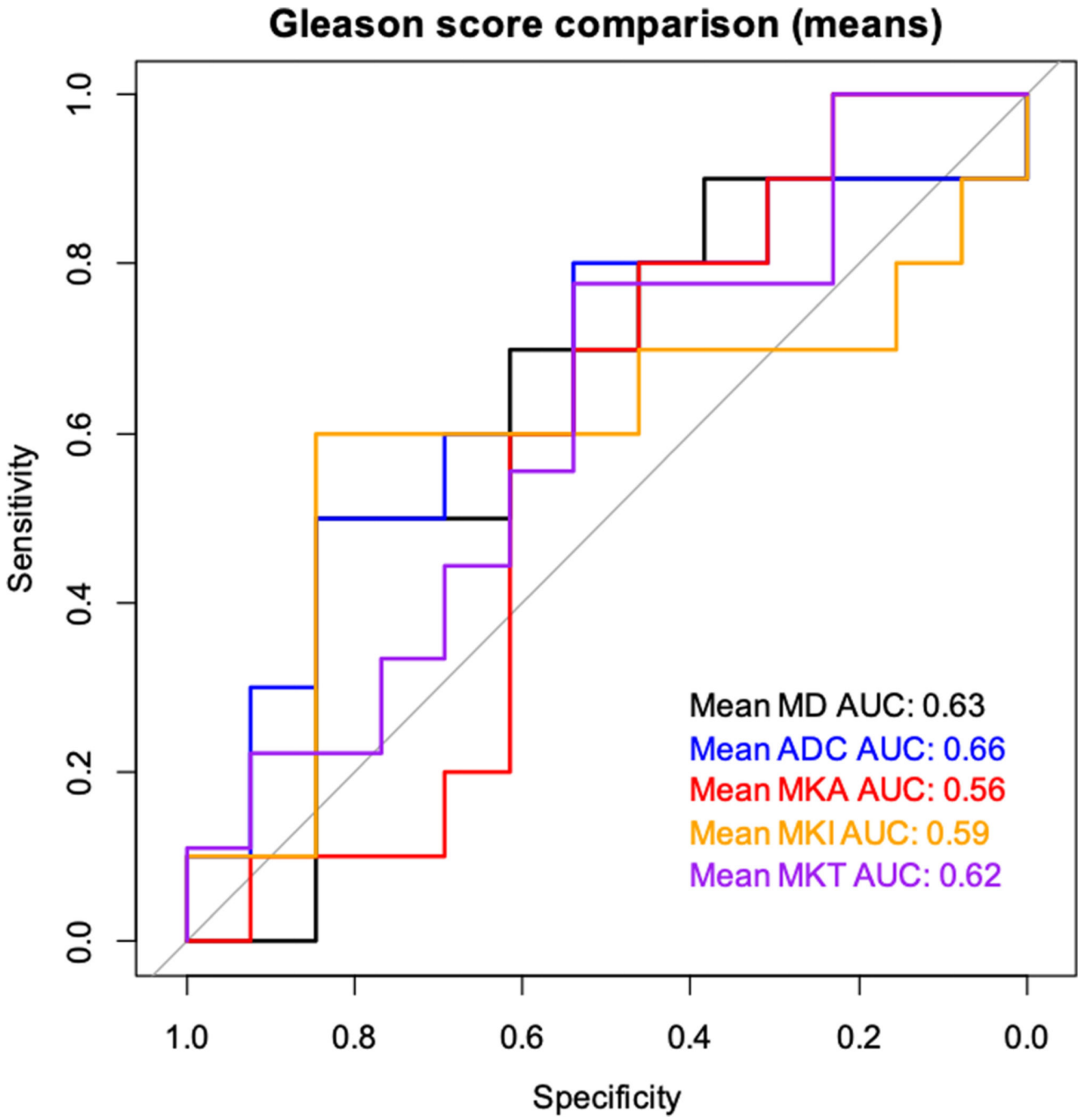

FIGURE 6.

ROC analysis using AUC for both ADC and MddMRI parameters (MD, MKa, MKi) in differentiating nonclinically significant (Gleason score 6, Gleason grade group 1) from clinically significant (Gleason score ≥7, Gleason grade group 2–4) prostate cancer. ROC indicates receiver operating characteristic curve; AUC, area under the curve; and ROI, normal region of interest.

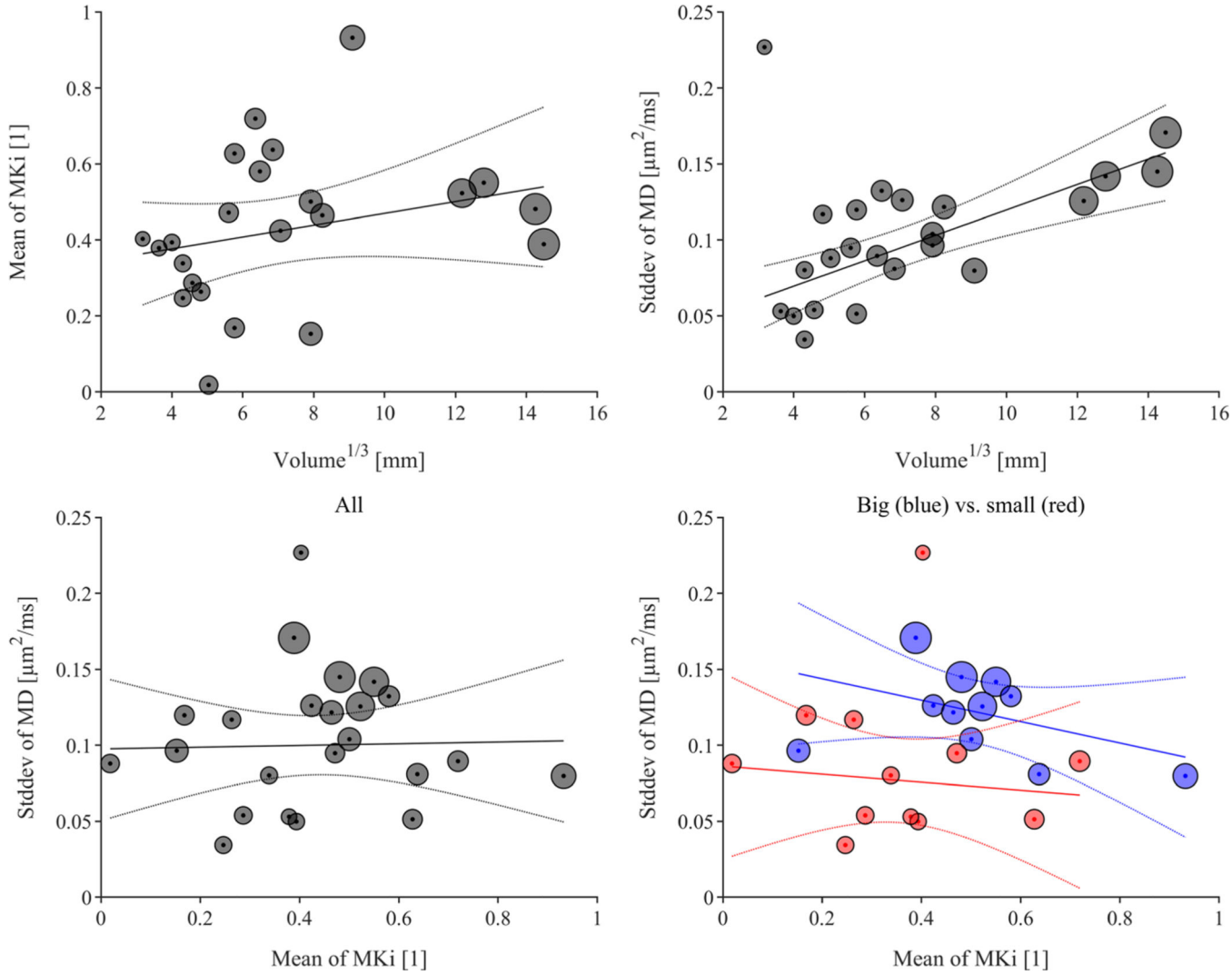

FIGURE 7.

Top row (A and B) outlines associations between tumor volume and microscopic diffusion heterogeneity and macroscopic diffusion heterogeneity. There was no significant correlation between tumor volume and microscopic diffusion heterogeneity (A, $P = 0.2$), whereas there was a significant correlation between tumor volume and macroscopic heterogeneity (B, $R^2 = 0.50$, slope = 0.008 µm^2/ms per millimeter, $P < 0.001$). Bottom row (C and D) outlines association between macroscopic diffusion heterogeneity and microscopic diffusion heterogeneity for all tumors (C), and when dichotomized by median volume into larger (red) and smaller (blue) tumors (D). No significant correlations were found between macroscopic and microscopic diffusion heterogeneity for all tumors evaluated together (C, $P = 0.9$) or when evaluated separately for small and big tumors (D, $P = 0.7$ and $P = 0.2$, respectively). MKi indicates microscopic diffusion heterogeneity; SD of MD indicates macroscopic diffusion heterogeneity.

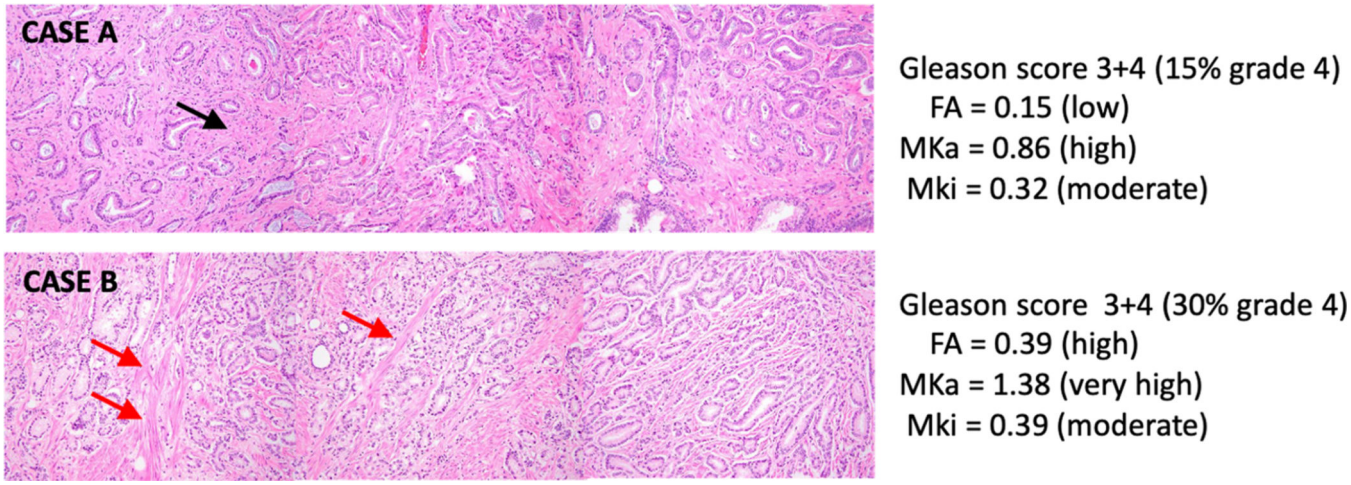

FIGURE 8.

Pictorial example of how the morphological components on histology in 2 different tumors of the same grade can be reflected in quantitative MddMRI measurements. Two RP cases with similar MKi, elevated and slightly different MKa, and markedly different FA (indicative of different levels of macroscopic anisotropy), and their corresponding morphological findings. Top 2 rows are hematoxylin-eosin–stained sections. Their corresponding Gleason score, FA, MKa, and MKi values are displayed in the table below. Case A is a mix of multidirectional, ill-defined stroma (black arrow) and neoplastic glandular structures. At the voxel level, the anisotropic microscopic features are randomly oriented, which may explain the low FA (ie, diffusion being close to isotropic). However, at the level of individual cells (ie, the microscopic level), it is possible that diffusion may occur predominantly along 1 direction, with a resultant high MKa. The moderately elevated MKi reflects the presence of nonuniformity of tissue diffusion at the microscopic level, that is, a mixture of luminal space with almost unhindered diffusion, glandular tissue with moderately hindered diffusion, and large amounts of stromal tissue with markedly hindered diffusion. Case B demonstrates a more moderate amount of stroma, which appears more well organized over longer distances along 1 direction, that is, fascicular (red arrows), thus both FA and MKa are higher. The higher MKa in case B may indicate slightly different architecture at the cellular level as well. As in case A, the tissue architecture variety appears relatively evenly distributed between luminal space, glandular cells, and stromal cells, thus MKi is moderately elevated. Abbreviations: GP, Gleason pattern; FA, fractional anisotropy; MKa, microscopic tissue anisotropy; MKi, microscopic diffusion heterogeneity. Note: Final Gleason score is based on evaluation of the entire RP, but only select hematoxylineosin–stained images are shown and may not represent the final Gleason score.

TABLE 1.

Patient Demographics

Patient Characteristics	No Tumor	PCa Confirmed	*P*	All Patients
No. patients	23	23		46
Age, y	67.0 (59.0, 69.0)	68.0 (61.0, 70.0)	0.49	67.0 (61.0, 69.0)
PSA, ng/mL	5.68 (4.66, 9.57)	4.98 (4.27, 7.90)	0.71	5.38 (4.33, 8.08)
PSA density, ng/mL^2	0.09 (0.07, 0.13)	0.12 (0.08, 0.21)	0.07	0.10 (0.08, 0.16)
Prostate gland volume on MRI, T2-weighted image, mL	62.0 (45.20, 88.0)	45.0 (35.10, 66.0)	0.018	55.0 (37.30, 72.0)
Tumor stage at RP (n = 7)				
pT2		n = 5/7		
pT3		n = 2/7		
Highest Gleason score (on biopsy or RP)				
3 + 3 = 6		10		
3 + 4 = 7		10		
4 + 3 = 7		2		
4 + 4 = 8		1		
MR-based tumor ROI: voxel volume/count				
MddMRI		16 mm^3/16.0 (6.0, 35.0)		
DWI		23 mm^3/13.0 (4.0, 41.0)		

Values are reported as the number of patients in each group or the parameter median with the interquartile range in parenthesis. *P* values obtained using Wilcoxon rank sum tests, comparing those with PCa to those with no tumor identified.

PCa, prostate cancer; PSA, prostate-specific antigen; MRI, magnetic resonance imaging; RP, radical prostatectomy; MddMRI, multidimensional diffusion magnetic resonance imaging; DWI, diffusion-weighted imaging.

TABLE 2.

Measures of Macroscopic and Microscopic Heterogeneity

Variable	Normal ROI, PZ	Normal ROI, TZ	Tumor ROI
MD, $\mu m^2/ms$			
Median	1.78	1.38	1.07
Interquartile range	1.52, 1.89	1.35, 1.56	0.82, 1.30
P *			<0.0001
MD (SD)			
Median	0.13	0.12	0.11
Interquartile range	0.08, 0.15	0.10, 0.15	0.08, 0.13
P *			NS
MKi			
Median	0.20	0.32	0.40
Interquartile range	0.18, 0.25	0.27, 0.36	0.29, 0.52
P *			0.0001
MKa			
Median	0.20	0.37	0.55
Interquartile range	0.15, 0.28	0.25, 0.41	0.36, 0.81
P *			<0.0001

Comparison of MddMRI-derived parameters in distinguishing tumor ROIs from normal ROIs.

* Friedman test P value.

Normal ROI PZ, normal region of interest within peripheral zone of prostate; normal ROI TZ, normal region of interest within transitional zone of prostate; tumor ROI, tumor region of interest.